DOI 10.1007/s10946-022-10092-9
Journal of Russian Laser Research, Volume 43, Number 6, November, 2022

EFFECT OF NONEQUILIBRIUM ELECTRON-ENERGY DISTRIBUTIONS ON EFFICIENCY OF RYDBERG STATE POPULATION VIA RESONANT RECOMBINATION

K. S. Kislov, A. A. Narits, and V. S. Lebedev*

Lebedev Physical Institute, Russian Academy of Sciences
Leninskii Prospect 53, Moscow 119991, Russia

*Corresponding author e-mail: vlebedev@sci.lebedev.ru

Abstract

We study how the efficiencies of resonant electron–ion recombination processes in rare-gas-mixture plasmas depend on the deviation of the electron-energy distribution functions from the Maxwellian distribution. Our calculations demonstrate that nonequilibrium distributions commonly encountered in the experiment may lead to strong increases or decreases of the respective rate constants of three-body and dissociative recombination processes. The dependences of the results on the electronic temperature and on the principal quantum number of the Rydberg state in the final channels of the reactions are analyzed.

Keywords: electron–ion recombination, nonequilibrium plasma, Rydberg atoms, resonant processes.

1. Introduction

Electron–ion recombination is one of the fundamental processes in plasma physics. It plays important roles in stellar and planetary atmospheres [1, 2], physics of gas, plasma and chemical lasers [3], astrophysics [1] and organic chemistry [4]. Recombination is a crucial component of kinetic models of plasma charge and excitation relaxation dynamics. Since the recombining electrons mainly populate the excited and highly-excited states of atoms or molecules, it is frequently utilized when achieving the population inversion; in particular, in the so-called recombination lasers [5]. So it is not surprising that the electron–ion recombination is currently a subject of intense experimental [6] and theoretical [4, 7] studies.

When a system comprised of the recombining electron, an atomic or molecular ion, and possibly a third particle or a light quantum features a channel of a resonant energy exchange between the electron and some internal degree of freedom, the rate of recombination may increase by many orders of magnitude. A good example of such a resonant mechanism is the process of dissociative recombination, which, due to the efficient energy exchange between the outer electron and the electronic shell of the molecular ion, may become a dominant recombination channel even in plasmas containing very small concentrations of molecular cations [8]. In our recent works [9, 10], we studied in detail the other resonant electron–ion recombination process, namely, electron capture to excited states of atoms in ternary collisions of electrons with ions A^+ and neutral atoms B. The process realizes due to the nonadiabatic transitions between the electronic terms of a quasimolecular system $A^+ + B + e$ temporary formed during the ternary collision. It was shown that, for quasimolecular ions with small dissociation energies, the resonant ternary electron capture may prevail over dissociative recombination.

Manuscript submitted by the authors in English on September 29, 2022.

1071-2836/22/4306-0653

Being essentially a rearrangement process and often a many-body process, electron–ion recombination is not an easy subject of study for both theory and experiment [1]. Owing to this, when the kinetic models of relaxation of various astrophysical and laboratory plasmas are developed, the role of recombination is mainly described using approximate expressions for rate constants based on either the results of the analysis of the experimental data, or some known theoretical data [11]. These rate constants, especially the ones obtained from the calculations, almost always imply that, in the plasma studied, the motion of free electrons and heavy particles obeys the local thermodynamical equilibrium (LTE) conditions; although often with different temperatures of electrons T_e and gas of heavy particles T. Then spread of the relative velocities of the electrons is described using the Maxwell distribution, while the population of the states of internuclear motion obeys the Boltzmann statistics in bound states and the Maxwell distribution in the continuum. Since the evaluation of the electronic energy distribution functions (EEDFs) and the distributions over the energy states of the nuclear motion is not a trivial task, the data obtained for the equilibrium conditions is frequently used in the collisional-radiative kinetic models [11,12] of the systems, for which the applicability of LTE-based results is not clear.

The aim of this work is to study the influence of nonequilibrium distributions of free electrons over the kinetic energy on the dynamics of the resonant recombination reactions. We consider the cases of the low-temperature plasmas of rare gas mixtures and the so-called merged beams setup often used in the studies of electron–ion recombination. For some nonequilibrium distributions typical of some standard experimental setups, we calculate the rate constants and cross sections averaged over the populations of the rovibrational states of the molecular cations. We compare the results to those obtained using the Maxwell distribution. We demonstrate that the nonequilibrium conditions may lead to changes in the resonant recombination-rate constants of up to two orders of magnitude. They may also have a pronounced effects on the relative roles of the reaction channels.

The theoretical calculations are based on a recently developed theoretical approach [9,10,13]. Unlike traditional theoretical methods used in recombination process studies, the approach is applicable to the situations, where a huge number of rovibrational states and a substantial part of the continuum of the states of internuclear motion in a (quasi)molecular ion gets populated. It allows one to quickly obtain the integral collisional properties describing the contributions of all the participating states. This is particularly convenient for the modeling of the plasma-based electromagnetic radiation sources [14,15].

This paper is organized as follows.

In Sec. 2, we briefly mention some types of the nonequilibrium plasma distributions deviating from the Maxwell–Boltzmann one and discuss in detail the specific distributions considered in this work. Basic formulas of the theoretical approach used are given in Sec. 3. The results of calculations are presented in Sec. 4. Finally, a brief summary of the results obtained is given in Sec. 5.

2. Nonequilibrium Energy Distributions of Electrons

Strictly speaking, each laboratory plasma device is characterized by its own specific electron-energy distribution and the distributions of the heavy particles over the bound and continuous states. When a plasma features different heavy particle components, with the possible chemical reactions between them, the distribution of the plasma constituents over the energy states is also likely to be different. It should also be noted that, for molecular species, the vibrational, rotational, and translational motions are often characterized by individual distribution functions. Obtaining these properties is, in most cases, a very difficult task requiring the numerical solution of kinetic Boltzmann equation or, in some simplified

situation, the Fokker–Planck equation. In practice, however, the complex kinetics of the nonequilibrium plasma is mainly described, using model approaches.

The model distributions are based on the assumptions of the predominance of one or another energy relaxation processes under specific plasma conditions. For example, one of the fundamental models is the two-temperature plasma approximation describing the electrons and the heavy particles by the Maxwell–Boltzmann distributions with different electron T_e and gas T temperatures. It presumes that the plasma heating primarily affects the electrons, which then quickly thermalize in electron–electron collisions owing to identical masses. In contrast, the heating of the neutral gas particles by collisions with electrons is very slow due to huge mass difference, so heavy particles are frequently characterized by ambient temperature. Below, we discuss some specific model electron-energy distributions currently used in the analysis of the experimental data.

2.1. Druyvesteyn Distribution

The Druyvesteyn distribution is a steady state solution of the Fokker–Planck equation for the electron diffusion in the energy space in the presence of constant electric field,

$$\frac{\partial f(\varepsilon)}{\partial t} = \frac{\partial}{\partial \varepsilon}\left[D_\varepsilon \frac{\partial f(\varepsilon)}{\partial \varepsilon} - f(\varepsilon) u_\varepsilon\right], \tag{1}$$

where $f(\varepsilon)$ is the distribution of electron energy ε. The first term on the right-hand side of the equation represents the diffusion process of electron motion in the energy space characterized by the diffusion coefficient

$$D_\varepsilon = \frac{1}{3}(m_e v_e u)^2 \nu_{en} = \frac{2}{3} m_e u^2 \varepsilon \nu_{en}. \tag{2}$$

Here, m_e and v_e are the electron mass and velocity, ν_{en} is the frequency of the electron neutral collisions and u is the additional velocity received by electron between collisions due to its drift in the electric field [16],

$$\vec{u} = -\frac{e\vec{E}}{m_e \nu_{en}}. \tag{3}$$

The second term on the right-hand side of the Fokker–Planck equation (1) represents the drift in the energy space due to the average energy gain and losses. The corresponding value – the electron drift velocity along the energy spectrum u_ε – is presented as [16]

$$u_\varepsilon = \left[\frac{m_e u^2}{2} - \frac{2m_e}{M}\varepsilon - P_{eV}(\varepsilon)\Delta E_V\right]\nu_{en}. \tag{4}$$

Here, the second term describes losses due to the elastic scattering on a heavy particle with mass M, while the third term describes loss due to the vibrational excitation of molecular species of plasma by electron impact characterized by the probability $P_{eV}(\varepsilon)$. When the energy losses in collisions with neutral particles are negligible, as compared to elastic electron–electron collisions, the steady-state solution of (1) for constant electron neutral collision frequency $\nu_{en} = \text{const}$ has the form of the standard Maxwell distribution with effective electron temperature T_e depending on the electric field,

$$k_\mathrm{B} T_e = \frac{e^2 E^2 M}{3 m_e^2 \nu_{en}^2}. \tag{5}$$

On the other hand, if the electron mean free path $\lambda = v_e/\nu_{en}$ is taken as constant, the solution is described by the Druyvesteyn distribution,

$$f(\varepsilon) = B \exp\left[-\frac{3m_e}{M}\frac{\varepsilon^2}{(eE\lambda)^2}\right]. \tag{6}$$

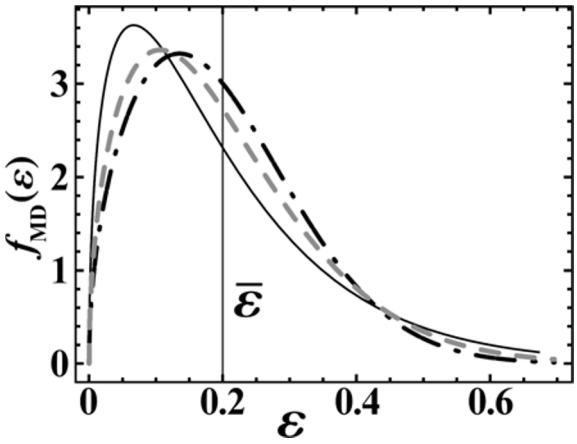

Fig. 1. Comparison of distributions over electron energies; here, the Maxwell distribution (the solid curve), the Druyvesteyn distribution (the dash-dotted curve), and general distribution $f_{\rm MD}(\varepsilon)$ Eq. (8) (the dashed curve).

Since both the Maxwell and Druyvesteyn distributions are two types of solutions of the Fokker–Planck equation (1) obtained for the same magnitude of the electric field, their influence over the efficiency of the recombination processes can be directly compared. Despite the fact that Eq. (6) is a nonequilibrium distribution, it is convenient to parameterize it, using effective electron temperature T_e given by (5) related to the mean electron energy of the distribution via $3k_{\rm B}T_e/2 = \phi$. As is seen from Eqs. (5) and (6), the value of $f(\varepsilon)$ strongly depends on parameters of the individual experimental setups, such as electric field, type of neutral particles, and their concentration. The introduction of values T_e and ϕ will allow us to obtain general results without need to substitute parameters of specific setups. For the case of Druyvesteyn distribution, the resulting equation expressed in terms of values T_e and/or ϕ reads [16]

$$f_{\rm D}(\varepsilon) = \frac{2\sqrt{\varepsilon}}{\phi^{3/2}} \cdot \frac{\Gamma(5/4)^{3/2}}{\Gamma(3/4)^{5/2}} \cdot \exp\left[-\left(\frac{\Gamma(5/4)}{\Gamma(3/4)} \cdot \frac{\varepsilon}{\phi}\right)^2\right], \tag{7}$$

where Γ is the Euler Gamma-function. As compared to the Maxwell distribution, $f_{\rm D}(\varepsilon)$ is smaller in the range of $\varepsilon \ll k_{\rm B}T_e$ and exhibits a much faster decline at high ε; see Fig. 1.

The Druyvesteyn distribution is often realized in weakly-ionized plasmas of atomic gases, including the plasmas of discharges in rare gases. It is also used as an approximation for $\varepsilon \to \infty$ limiting case of EEDFs observed under various discharge conditions, where the energy tail of the EEDF is rapidly depleted.

In the interpretation of the experimental data, a more general form of $f(\varepsilon)$ is commonly used [17]; it is

$$f_{\rm MD}(\varepsilon) = \frac{c_1\sqrt{\varepsilon}}{\phi^{3/2}} \exp\left[-c_2\left(\frac{\varepsilon}{\phi}\right)^x\right], \qquad c_1 = x\frac{(\Gamma(5/2x))^{3/2}}{(\Gamma(3/2x))^{5/2}}, \qquad c_2 = \left[\frac{(\Gamma(5/2x))}{(\Gamma(3/2x))}\right]^x, \tag{8}$$

where $x \in [1, 2]$. One can see that, at $x = 2$, Eq. (8) coincides with Eq. (7), whereas at $x = 1$ it reduces to the Maxwell distribution. The value of x is then determined by the fitting of the experimental results. In Fig. 1, we show $f_{\rm DM}(\varepsilon)$ for several values of x.

2.2. Distribution of Cooled Merged Beams

The technique of merged beams is a powerful experimental method, whereby two particle beams share a common interaction path. It provides exceptional energy resolution at low center of mass energies.

While not being a plasma, it is one of the most precise method of measuring the rates and cross sections of various recombination processes when combined with ion storage rings [1,18]. Thus, correct description of the role of the nonequilibrium electron energy distributions in the efficiency of elementary processes in the electron–ion collisions measured in merged beams is crucial for the modeling of plasma kinetics.

Coulomb interaction between ions and electrons in the merged beams acts as a friction force for the ions with velocities different from the mean velocity of the beams, resulting in a very high quality of the ionic beam. In the reference frame of the ionic beam, the velocities of the electrons are then characterized by the anisotropic Maxwellian distribution [1,18],

$$f(v_e, v_d) = [m_e/(2\pi k_{\rm B} T_\perp)] \exp\left[-m_e v_\perp^2/(2k_{\rm B}T_\perp)\right] \sqrt{m_e/(2\pi k_{\rm B} T_{||})} \exp\left[-m_e(v_{||} - v_d)^2/(k_B T_{||})\right], \quad (9)$$

with $v_{||}$ and $v_\perp$ being the components of electron velocity v_e aligned parallel and perpendicular to the ionic beam direction, respectively, and $v_{\rm d}$ is the so-called detuning velocity determined by the voltage applied in the interaction region. The effective temperature $T_\perp$, characterizing the motion of electrons in the transverse x, y plane, is usually associated with the regular electronic temperature T_e. This is the temperature, electron cloud has after being formed in front of a cathode, and it takes values of $k_{\rm B}T_\perp \sim 0.1$ eV. Temperature $T_{||}$ characterizes the motion of electrons in the longitudinal z direction of the merged-beam setup. The velocity distribution in this direction is significantly reduced compared to the x and y directions due to the kinematic compression effect [1], so that the value $k_{\rm B}T_{||}$ may be as low as 0.1 meV. Moreover, the longitudinal velocity distribution is centered around the so-called detuning velocity $v_{\rm d}$, which is equal to the difference between the electron and ion speeds in the z direction. The electron velocity distribution (9) is controlled by the variation of the detuning energy, $E_{\rm d} = m_e v_{\rm d}^2/2$, in the range of $E_{\rm d} \in [0, 0.5]$ eV.

3. Theoretical Approach

In this work, we study the effect of nonequilibrium distributions of electrons and heavy particles on the rates of the resonant electron–ion recombination resulting in the electron capture to the Rydberg atomic states. The process is realized via two channels – the dissociative electron capture,

$$\mathrm{BA}^+(i, vJ) + e \to \mathrm{BA}(f, nl) \to \mathrm{A}(nl) + \mathrm{B}, \quad (10)$$

and resonant electron capture in ternary collisions of electrons, atomic ions, and neutral atoms,

$$\mathrm{A}^+ + e + \mathrm{B} \to \mathrm{BA}^+(i) + e \to \mathrm{BA}(f, nl) \to \mathrm{A}(nl) + \mathrm{B}. \quad (11)$$

Here, i and f denote the initial and final electronic terms of the (quasi)molecular ion BA^+, v and J are vibrational and rotational quantum numbers of the molecular ion in the initial electronic state, and n and l are the principal and orbital quantum numbers of the Rydberg state in the final channel of the reactions. Both processes (10) and (11) occur as a result of nonadiabatic transitions in $\mathrm{B}+\mathrm{A}^+ + e$ system. In the case of dissociative electron capture, the system initially populates a bound rovibrational state whereas, for the resonant ternary capture, the system is initially in the continuum of the internuclear motion.

According to the theory of nonadiabatic transitions [19], the transitions mostly occur in the vicinity of the crossing point R_ω of the electronic terms. For the resonant recombination processes (4) and (5)

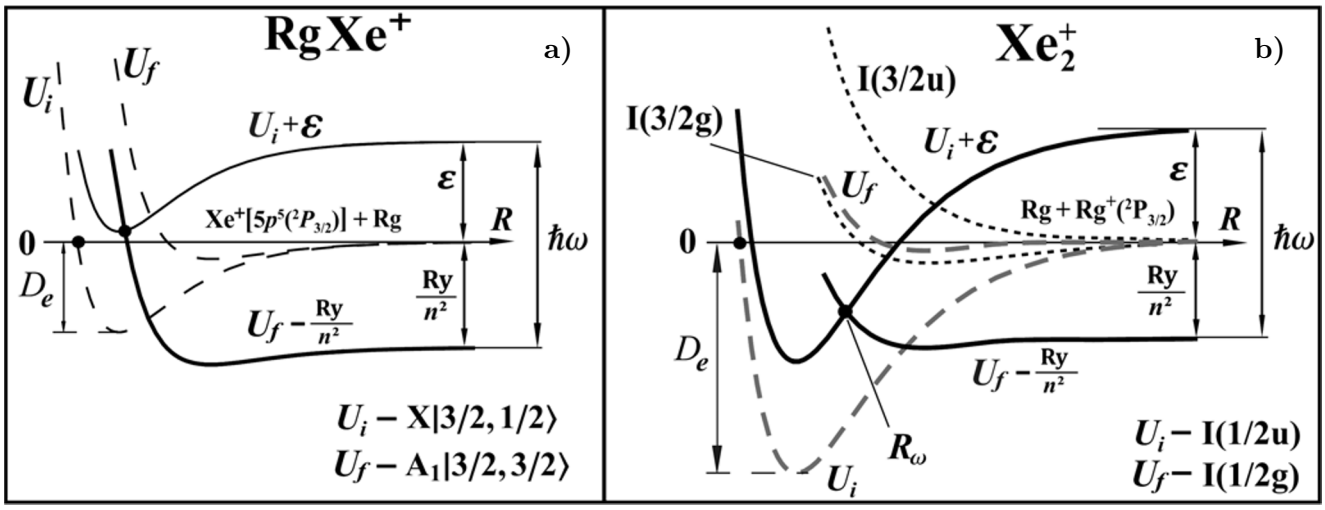

Fig. 2. Scheme of the nonadiabatic transitions resulting in the capture of electron from continuum with energy $\varepsilon > 0$ to a Rydberg n state with energy $-\mathrm{Ry}/n^2$ for the heteronuclear $\mathrm{Rg} + \mathrm{Xe}^+ + e$ system (a) and for the homonuclear $\mathrm{Xe} + \mathrm{Xe}^+ + e$ system (b).

under consideration, this yields [9, 10]

$$U_i(R_\omega) + \frac{\hbar^2 k^2}{2m_e} = U_f(R_\omega) - \frac{\mathrm{Ry}}{n_*^2}, \tag{12}$$

where $U_i(R)$ and $U_f(R)$ are the initial and final electronic terms of BA^+, respectively, $\dfrac{\hbar^2 k^2}{2m_e} = \varepsilon$ is the free electron energy before the collision, and $n_* = n - \delta_l$ is the effective principal quantum number of the Rydberg state. Also, we introduced the effective transition frequency $\omega = (\varepsilon + \mathrm{Ry}/n_*^2)/\hbar$ and the quantum defect δ_l of the atomic Rydberg state. The schematics of reactions (10) and (11) for cases of heteronuclear and homonuclear molecular ions are presented in Fig. 2.

Calculations of cross sections and rate constants of processes (10) and (11) carried out in this work are based on the theoretical approach developed in [9, 10, 13]. It is based on the quantal variant of the theory of nonadiabatic transitions [20], the semiclassical approximation of the quasicontinuum of the rovibrational states and an effective technique, which reduces the summation over the rotational and vibrational quantum numbers to the integration over quasicontinuous variables. According to [9, 10], the cross section of the capture of an electron with energy ε to the Rydberg nl state of atom A as a result of a nonadiabatic transition in the quasimolecular ion BA^+ with energy E temporary formed during the ternary collision (11) can be written as

$$\sigma^{\mathrm{tr}}_{\varepsilon\to nl}(E) = \tilde{g}_{\mathrm{tr}}(2l+1)\frac{4\pi^4 \Gamma_{nl\to\varepsilon}(R_\omega)\sqrt{2\mu}}{q^2 k^2 \Delta F_{fi}(R_\omega)} \int_0^\infty d(J^2)\sqrt{\xi_J(R_\omega)}\mathrm{Ai}^2\left[-\xi_J(R_\omega)\left(E - U_i^J(R_\omega)\right)\right] S_{nl}^J(R_\omega), \tag{13}$$

$$\xi_J(R_\omega) = \left(\frac{2\mu}{\hbar^2}\right)^{1/3}\left|\frac{\Delta F_{fi}(R_\omega)}{F_f^J(R_\omega)F_i^J(R_\omega)}\right|^{2/3}, \quad \Gamma_{nl\to\varepsilon}(R_\omega) = \frac{2\pi}{2l+1}\sum_{m,m'l'}\left|\mathrm{V}^{f,nlm}_{i,\varepsilon l'm'}(R_\omega)\right|^2. \tag{14}$$

Here, $E = \dfrac{\hbar^2 q^2}{2\mu}$ is the nuclei kinetic energy before the collision, $\tilde{g}_{\mathrm{tr}} = \dfrac{g_{\mathrm{BA}^+(f)}}{\mathfrak{s}\, g_{\mathrm{B}(i)} g_{\mathrm{A}^+(i)}}$ is the electronic

statistical weight, $\mathfrak{s}$ is a symmetry factor equal to 2 for homonuclear systems, if both U_i and U_f are Σ-terms, and equal to 1 otherwise, μ is the reduced mass of the nuclei, $\Gamma_{nl\to\varepsilon}(R)$ is the autoionization width calculated within the framework of the perturbation theory, $\mathrm{Ai}(x)$ is the Airy function, and $\Delta F_{fi}(R)$ is the difference between the slopes $F_i^J(R)$ and $F_f^J(R)$ of the potential energy curves $U_i^J(R_\omega)$ and $U_f^J(R_\omega)$, which also include the rotational energy $U_{i,f}^J(R) = U_{i,f}(R)+\hbar^2 J(J+1)/2\mu R^2$. Formula (13) contains also the so-called survival factor $S_{nl}^J(R_\omega)$ [9], which describes the probability for B + A(nl) not to undergo the inverse process of autoionization until it reaches the stabilization point, after which the backward process becomes forbidden by the energy conservation. However, for rare gas molecular ions considered in this work, the factor is close to unity.

The respective expression for the cross section of the dissociative recombination of BA^+ molecular ion in rovibrational state vJ with an electron with energy ε, leading to the population of Rydberg nl state of atom A in the final channel of the reaction, reads [9]

$$\sigma_{\varepsilon\to nl}^{\mathrm{dr}}(vJ) = \tilde{g}_{\mathrm{dr}} \frac{\mathfrak{s}\,(2l+1)4\pi^3\sqrt{2\mu}\Gamma_{nl\to\varepsilon}(R_\omega)}{T_{vJ}k^2\Delta F_{fi}(R_\omega)} \sqrt{\xi_J(R_\omega)}\mathrm{Ai}^2\left[-\xi_J(R_\omega)\left(E_{vJ}-U_i^J(R_\omega)\right)\right], \qquad (15)$$

where $\tilde{g}_{\mathrm{dr}} = \dfrac{g_{\mathrm{BA}^+(f)}}{\mathfrak{s}\, g_{\mathrm{BA}^+(i)}}$, E_{vJ} is the binding energy of rovibrational vJ-state, and T_{vJ} is the period of the classical motion with energy E_{vJ} in the potential well $U_i^J(R)$.

Equations (13) and (15) express the cross sections of the resonant ternary electron capture and dissociative electron capture in terms of the potential energy curves and their parameters, and the autoionization widths $\Gamma_{nl\to\varepsilon}(R)$. The evaluation of the latter quantities generally require the application of high-precision computational methods based on R-matrix approach [21] or the complex Kohn variational method [22]. For moderately bound molecular ions at room and elevated temperatures, this becomes prohibitively time consuming owing to the giant number of participating states. At the same time, when one is interested in the integral collisional properties like averaged cross sections or rate constants, it is possible to use model approaches based on the perturbation theory. In this work, we determined $\Gamma_{nl\to\varepsilon}(R)$ in the dipole approximation for homonuclear systems, whereas for heteronuclear systems a vacancy model [23] was utilized.

To obtain the rate constants of processes (10) and (11), one needs to average the cross sections (15) and (13) over the distributions of heavy particles over the rovibrational and continuum states, respectively, followed by averaging the results over the electron velocity distributions,

$$\alpha_{nl}^{\mathrm{dr}}(T_e,T) = \left\langle v_\varepsilon \sum_{vJ} f_T(vJ)\sigma_{\varepsilon\to nl}^{\mathrm{dr}}(vJ)\right\rangle_{f_{T_e}}, \qquad (16)$$

$$\beta_{nl}^{\mathrm{tr}}(T_e,T) = \left\langle v_\varepsilon \left\langle V_E \sigma_{\varepsilon\to nl}^{\mathrm{tr}}(E)\right\rangle_{f_T}\right\rangle_{f_{T_e}}. \qquad (17)$$

Here, f_{T_e} is the distribution of electron velocity v_ε corresponding to the electronic temperature T_e (when it is defined); $f_T(vJ)$ and f_T are the distributions of heavy particles over the rovibrational states, and the distributions of the heavy particles velocity V_E before the collision, corresponding to gas temperature T (when it can be introduced). In the experiments, one is usually interested in n dependences of the rate constants, whereas l dependences are often neglected (except for $l = 0-2$ when the quantum defect δ_l

is substantial). The rate constants can then be summed over l,

$$\alpha_n^{\rm dr}(T_e,T)=\sum_{l=0}^{n-1}\alpha_{nl}^{\rm dr}(T_e,T),\ \beta_n^{\rm tr}(T_e,T)=\sum_{l=0}^{n-1}\beta_{nl}^{\rm tr}(T_e,T). \tag{18}$$

When the electrons velocities and the internuclear motion obey the Maxwell and Maxwell–Boltzmann distributions, the averaging in (16) and (17) can be carried out semi-analytically in the quasicontinuum approximation. The respective formulas were obtained in [9,10]. In the case of nonequilibrium distributions of electron and/or internuclear motion, the rate constants should be evaluated numerically using equations (13)–(15) and (16) and (17).

4. Results of Calculations

We carried out specific calculations for plasmas of rare gas mixtures, Ar/Xe and Kr/Xe, under conditions typical of active media of gas lasers and discharge afterglows. Below, we present the results obtained for the rate constants of dissociative recombination $\alpha_n^{\rm dr}(T_e,T)$, resonant ternary electron capture $\beta_n^{\rm tr}(T_e,T)$, and total rate of resonant recombination $\beta_n^{\rm r}(T_e,T)$ of heteronuclear and homonuclear (quasi)molecular ions with electrons for the nonequilibrium distributions discussed above. It is important to note that, in the calculations carried out under conditions of the deviations from the equilibrium, the electronic temperatures T_e are described by the effective values as explained in Sec. 2. The respective values are also applicable in the limiting cases where the specific nonequilibrium distributions transform into the Maxwell distribution.

4.1. Druyvesteyn Distribution and Its Generalization

The ratios of the rates of resonant electron–ion recombination $\beta_n^{\rm r}(T_e,T)=\beta_n^{\rm dr}(T_e,T)+\beta_n^{\rm tr}(T_e,T)$ calculated, using generalized Druyvesteyn (Eq. (8), $x=2$ and $x=1.5$) and Maxwell distributions of the incident electron energies, are shown in Fig. 3. The data are presented for $KrXe^+$ ions (a and b) and $ArXe^+$ ions (c and d). It can be seen that the nonequilibrium distribution results in the change of both magnitudes of the rate constants and the shape of the rate constant profile. The behavior also substantially differs for different ions. For $KrXe^+$ at relatively low electronic temperatures T_e, the Druyvesteyn distribution of electrons leads to much more narrow profile in the n dependences of the rate constants, so that only a limited set of states near $n=10$ gets populated by the electron capture processes (10) and (11). The increase in T_e results in the profile broadening and the shift of the maximum positions towards higher n. One can see that generally the results obtained using $f_{\rm MD}(\varepsilon)$ are smaller for $x=2$ as compared to $x=1.5$, with the exception of data for $KrXe^+$ at $T_e=1500-2000\,$K. In the case of $ArXe^+$, the rate constants are significantly smaller for the Druyvesteyn distribution than for the Maxwell distribution, except for capture to states with very high n. Unlike $KrXe^+$, for $ArXe^+$ the ratios $\beta_{\rm Dryuv}^{\rm r}/\beta_{\rm Maxw}^{\rm r}(n,T_e,T)$ mostly increase with increase in n, and decrease with increase in T_e.

The behavior of the ratios in the low n part of the profile at medium T_e stems from the fact that the respective transitions mainly occur at $\varepsilon<\bar{\varepsilon}$ and, for such energies, the electron densities are lower for the Druyvesteyn distribution. The effect propagates to higher n at high temperatures owing to the form of the Druyvesteyn distribution and, at $T_e=10,000\,$K, it is almost uniform across all n.

The intermediate case of generalized Druyvesteyn distribution with $x=1.5$ generally exhibits the same behavior as $x=2$. This suggests that in (8) the principal role is played by the quick decline

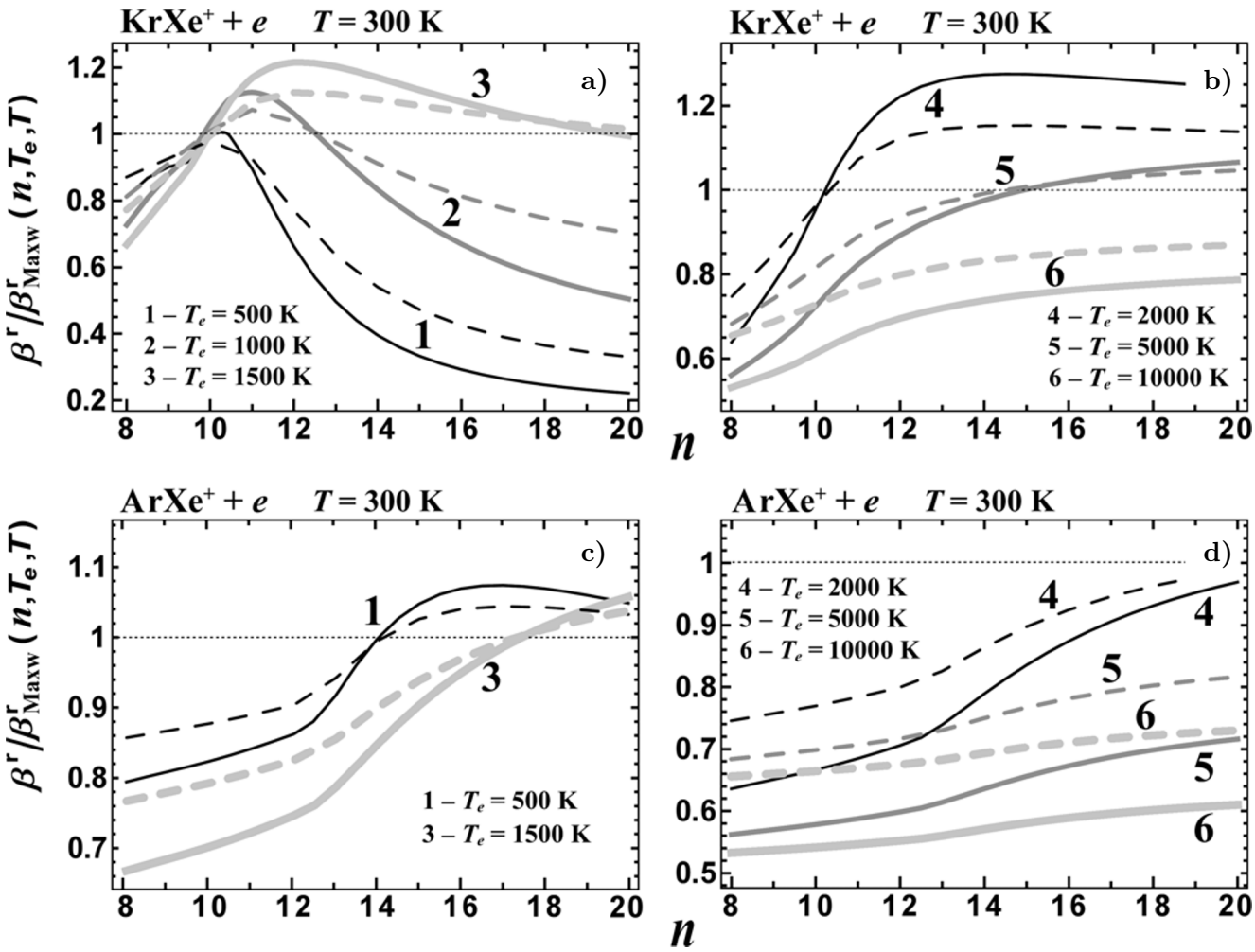

Fig. 3. The $\beta^{\mathrm{r}}/\beta^{\mathrm{r}}_{\mathrm{Maxw}}(n, T_e, T)$ ratios of the rates of resonant electron–ion recombination obtained at $T = 300\,\mathrm{K}$ and different T_e for $\mathrm{KrXe}^+ + e$ (a, b), and $\mathrm{ArXe}^+ + e$ (c) systems for generalized Druyvesteyn distribution at $x = 2$ (solid curves) and $x = 1.5$ (dashed curves) and Maxwell distribution (Maxw).

of high-ε tail of the distribution, while the decreased magnitudes of $f_{\mathrm{MD}}(\varepsilon)$ at low ε mainly affect the magnitudes of the ratios in Fig. 3 rather than the form of their n-variation.

Overall, one can see that the deviation of the electron-energy distribution from the equilibrium may strongly influence the dynamics of dissociative recombination and ternary electron capture in heteronuclear rare gas molecular ions, both in terms of the reaction rates, and in the magnitudes of the principal quantum numbers n of Rydberg states getting predominantly populated.

In Fig. 4 we present the results of calculations of $\beta^{\mathrm{r}}/\beta^{\mathrm{r}}_{\mathrm{Maxw}}(n, T_e, T)$ (the ratios of resonant recombination rates), resulting in the electron capture to Rydberg n-states, for homonuclear system $\mathrm{Xe}_2^+ + e$ obtained for generalized Druyvesteyn and Maxwell distributions. Owing to substantial dissociation energy of Xe_2^+ ion equal to 0.98 eV, the electron capture process is dominated by dissociative recombination. Here, it is important to stress that we consider only the recombination processes leading to population of highly-excited states. However, in the case of Xe_2^+, there is a strong contribution of the recombina-

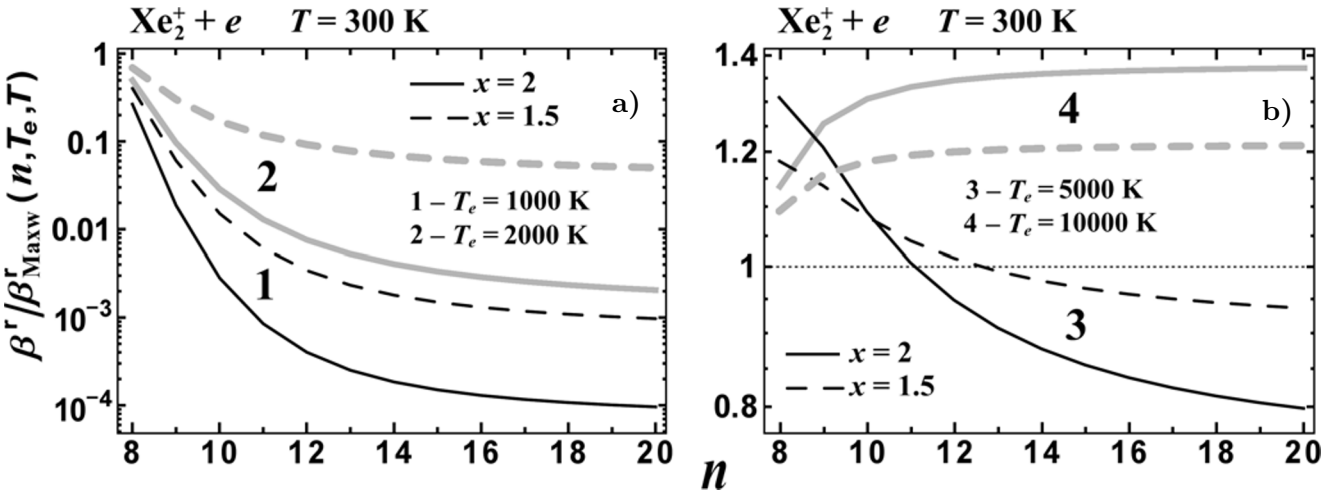

Fig. 4. The $\beta^{\rm r}/\beta^{\rm r}_{\rm Maxw}(n, T_e, T)$ ratios of the rates of resonant electron–ion recombination obtained at $T = 300\,{\rm K}$ and different T_e for $Xe_2^+ + e$ system for generalized Druyvesteyn distribution at $x = 2$ (solid curves) and $x = 1.5$ (dashed curves) and Maxwell distribution (Maxw).

tion resulting in electron populating the lowest excited states of Xe, which cannot be described by the theoretical approach used. Thus, the data in Fig. 4 are limited to relatively high values of n. Correct treatment of the electron capture to lower states requires extensive many-electron calculations, which are beyond the scope of the present work.

It is seen in Fig. 4 that, at $T_e \le 3000\,{\rm K}$, the results obtained with the Druyvesteyn distribution are orders of magnitude smaller than the data calculated with the Maxwell distribution. This is in accordance with the respective results for $KrXe^+$; see Fig. 3 a, although, since the maximum of the rate constant is in the small n region, there is no peak in Fig. 4 a. It is a consequence of rapid decline of high ε tail of $f_{\rm MD}(\varepsilon)$. Increase in T_e up to 5000 K changes the behavior of the ratios dramatically – distribution (8) now yields higher rate constants at low n, while, at high n, the Maxwell distribution gives somewhat higher values of $\beta^r(n, T_e, T)$. Similar to the change between Fig. 3 a and b, further increase in electronic temperature changes the n-dependence of $\beta^{\rm r}/\beta^{\rm r}_{\rm Maxw}(n, T_e, T)$ again, resulting in the ratios being in the range of 1.2 – 1.4 for the entire range of n considered.

As expected from the comparison with $KrXe^+$ ions, the intermediate case of $x = 1.5$ mostly follows the behavior of the rations for $x = 2$, with ratios being somewhat closer to unity.

Data shown in Fig. 4 suggest that, for homonuclear ions, the rate constants of resonant recombination (mostly dominated by dissociative recombination) turn out to be even more sensitive to the deviation of the EEDFs from those given by the Maxwell distribution. Depending on the magnitude of the electronic temperature, the resulting rate constants may either decrease by orders of magnitude or increase by up to 40%. The drastic changes in the dependences of the rate constants on n are crucial when the recombination is used to populate the upper levels of working transitions in powerful gas lasers.

4.2. Velocity Distribution in Merged Beams

In this section, we present the results of calculations obtained using anisotropic Maxwell distribution of the electron velocities typically realized in the experiments, where the technique of cooled merged beams is utilized; see Sec. 2.2. The velocity distribution is varied using detuning energy E_d, Eq. (9). In

Fig. 5, we show the dependences of the rate constant of dissociative recombination of $ArXe^+$ (a) and $KrXe^+$ (b) ions with electrons on the value of the principal quantum number of Rydberg atom in the final channel of reaction (10). The results were calculated for $T_e = 3000$ K, $T = 400$ K and 900 K (the dashed curve, Maxwell distribution) and for merged beams distributions with $E_d = 0.1$, 0.2, 0.3, 0.4, 0.5 eV (curves 1–5, respectively). One can see from the data presented that $\alpha_n^{\rm dr}(T_e, T)$ is quite sensitive to the variation of the EEDFs: for $ArXe^+$, increase in E_d to 0.3 eV decreases the value of the rate constant at maximum by 30 times. It also shifts the position of the maximum from $n = 12$ to $n = 15$. In the case of

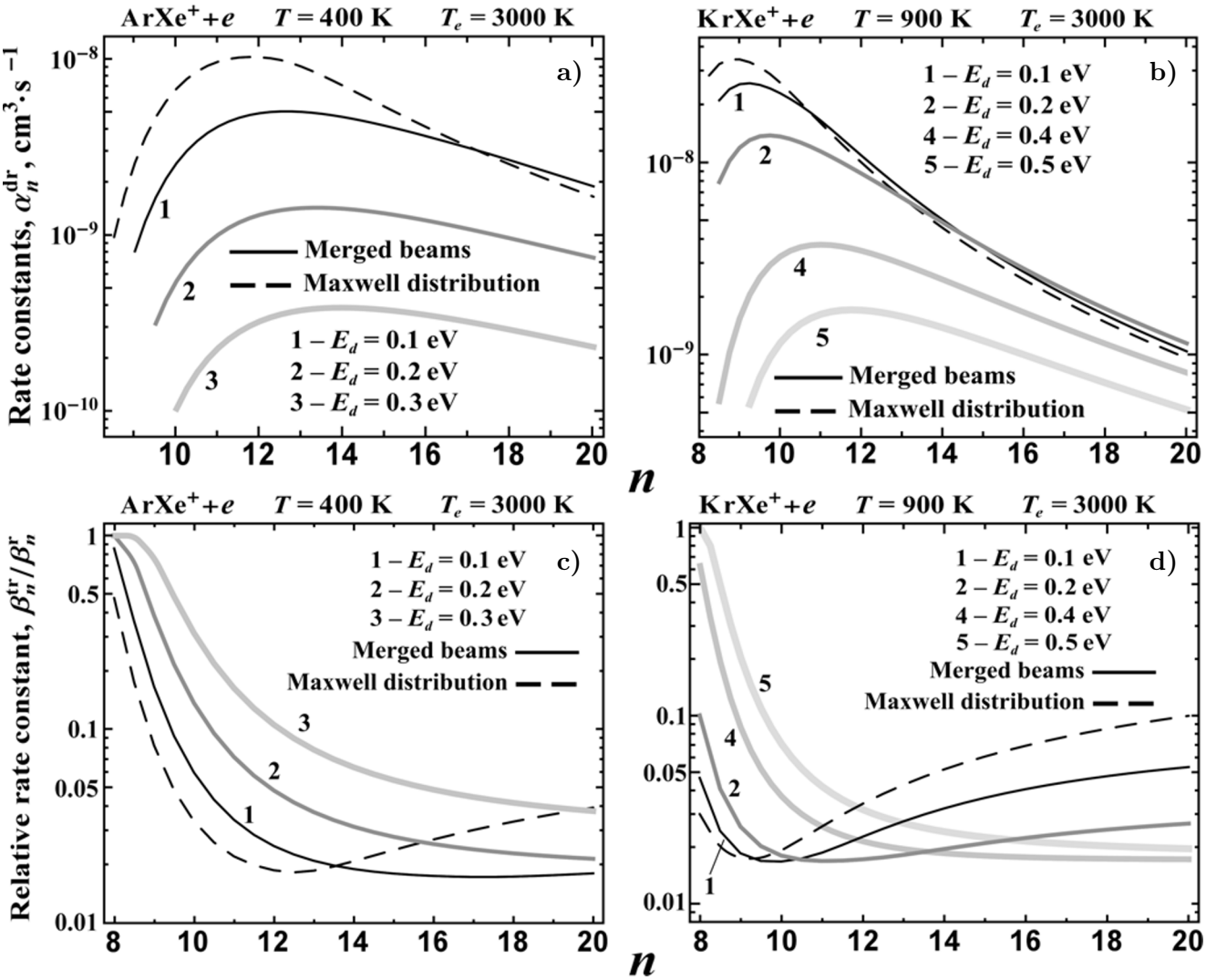

Fig. 5. Rate constants $\alpha_n^{\rm dr}(T_e, T)$ [cm^3·s^{-1}] of dissociative recombination leading to the population of atomic Rydberg states for $ArXe^+$ (a) and $KrXe^+$ (b) ions obtained, using the Maxwell distribution (dashed curves) and anisotropic Maxwell distribution (realized in setups with merged beams) of electron energy. Relative contributions $\beta_n^{\rm tr}/\beta_n^{\rm r}(n, T_e, T)$ of resonant ternary electron capture into the total rate of resonant electron–ion recombination as functions of the principal quantum number of the Rydberg state getting populated for $Ar{+}Xe^+ + e$ (c) and $Kr{+}Xe^+ + e$ (d) systems calculated, using the Maxwell distribution and merged-beam distribution of incident electron energy. The calculations were done with detuning energies of $E_d = 0.1 - 0.5$ eV, $T_e = 3000$ K, $T = 400$ K ($ArXe^+$) and 900 K ($KrXe^+$).

$KrXe^+$, the effect is somewhat weaker but still exceeds an order of magnitude, when E_d is increased to 0.5 eV.

One can also note that merged-beam distribution function may allow for more effective population of states with higher n. Not only increase in E_d shifts the position of the maximum of $\alpha_n^{\rm dr}(T_e, T)$ towards higher n but also, at small E_d, the distortion of the EEDF increases the magnitude of $\alpha_n^{\rm dr}(T_e, T)$ as compared to those calculated, using the Maxwell distribution.

In Fig. 5 c, d, we show the relative contribution of the ternary resonant electron capture process (11), alternative to dissociative recombination (10), to the total rate of resonant recombination. In the case of Maxwellian distribution, $\beta^{\rm tr}_{\varepsilon\to n}(T_e, T)/\beta^{\rm r}_{\varepsilon\to n}(T_e, T)$ exhibits a minimum near the location of the maximum of $\beta^{\rm r}_{\varepsilon\to n}(T_e, T)$, so that the contribution of the ternary capture can be neglected. The introduction of detuning voltage increases $\beta^{\rm tr}_{\varepsilon\to n}(T_e, T)/\beta^{\rm r}_{\varepsilon\to n}(T_e, T)$ by up to 5 times depending on E_d. As a result, the resonant ternary capture process yields up to 10% of the resonant recombination at the position of the maximum. The effect is stronger for ions with smaller dissociation energies. The deviation of the electron distribution from the equilibrium also changes the dependence of the ratio on n – at high E_d, the ratio of $\beta^{\rm tr}_{\varepsilon\to n}(T_e, T)/\beta^{\rm r}_{\varepsilon\to n}(T_e, T)$ monotonically decreases with increase in n.

For homonuclear ions, the situation is different; see Fig. 6. Small detuning energy (0.1 eV) results in the slight decrease of the rates of dissociative recombination of Xe_2^+ with electrons owing to rather complex structure of the respective EEDF. Increase in E_d has an opposite effect – the spread of the electron energy distribution allows for more efficient population of Rydberg states with higher n, so that $\alpha_n^{\rm dr}(T_e, T)$ calculated with the merged-beam distribution function becomes greater than that calculated using the Maxwell distribution at all n shown in Fig. 6 a. The drastic change in the effect of the nonequilibrium distribution as compared to $RgXe^+$ ions reflects the fact that, with much higher D_0 of Xe_2^+, the dissociative recombination process (10) mainly populates the lowest excited states of Xe I, while we only consider the electron capture to Rydberg states. Thus, the dependences presented in Fig. 6 a

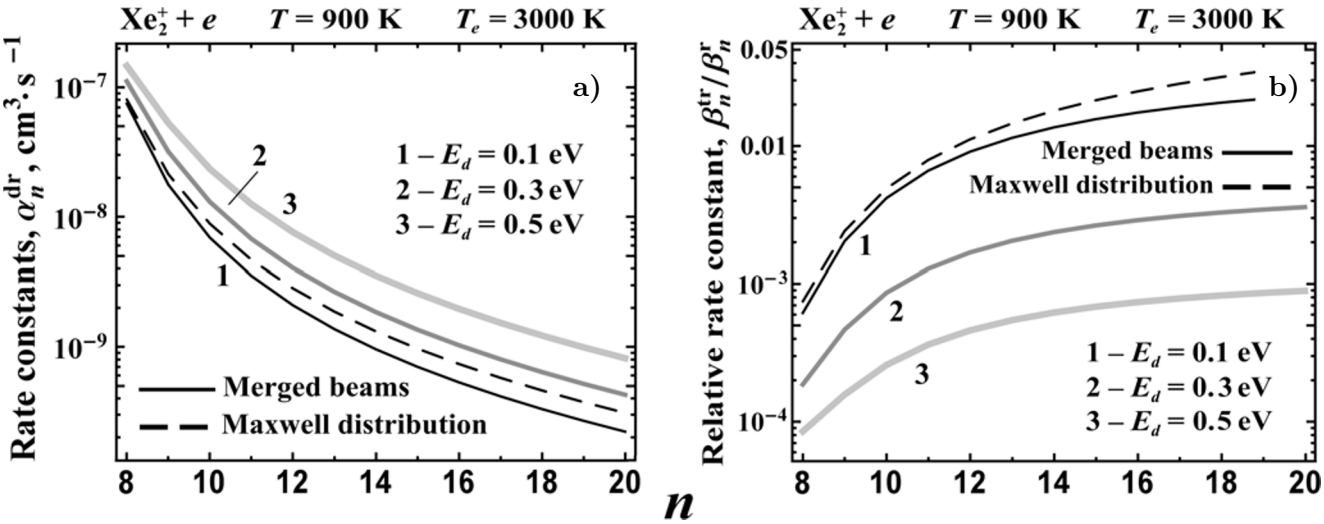

Fig. 6. The dependences of rate constants $\alpha_n^{\rm dr}(T_e, T)$ [cm$^3\cdot$ s^{-1}] of dissociative recombination of Xe_2^+ with electrons leading to population of atomic Rydberg states on n (a) calculated using the Maxwell distribution and anisotropic Maxwell distribution (9). Relative contributions $\beta_n^{\rm tr}/\beta_n^{\rm r}(n, T_e, T)$ of resonant ternary electron capture into the total rate of resonant electron–ion recombination as functions of the principal quantum number of the Rydberg state getting populated for $Xe{+}Xe^+ + e$ system at $T_e = 3000$ K, $T = 900$ K, and $E_d = 0.1$, 0.3, and 0.5 eV (b).

should be compared with the high n wings of the respective curves in Fig. 5 a, b. Then one can see some similarity between the curves shown in Fig. 6 a and Fig. 5 b. Nevertheless, there are some considerable differences in the behavior of $\alpha_n^{\rm dr}(T_e, T)$ calculated for Xe_2^+ and $KrXe^+$ even at high n. These stem from the specifics of the potential energy curves of homonuclear and heteronuclear rare gas ions.

The dependences of the contribution of the resonant ternary electron capture process in the total rate of resonant recombination on the magnitude of the detuning energies (Fig. 6 b) are also alike to the high n part of the respective graphs obtained for $KrXe^+$; see Fig. 5 d. The difference between $\beta_{\varepsilon\to n}^{\rm tr}(T_e, T)/\beta_{\varepsilon\to n}^{\rm r}(T_e, T)$ calculated using the Maxwell distribution and the EEDF typical of setup of merged beams exceeds an order of magnitude in the favor of the former. From the comparison of Figs. 5 d and 6 b, we expect that, for the resonant recombination of Xe_2^+ with electrons at low n, the role of the ternary electron capture mechanism will be substantial.

5. Summary

We demonstrated that the deviation of the electron-energy distribution functions from the equilibrium expression given by the Maxwell distribution might have a strong impact on the efficiency of the resonant electron–ion recombination. In the case of Druyvesteyn distribution often realized in rare gas plasmas, we found that for molecular ions with moderate dissociation energies in the regime of small electron temperatures the n-profile of the rate constant became much more narrow favoring the population of a very limited set of excited states of Xe I. This is important for the modeling of the kinetics of population inversion in powerful Xe I lasers. In contrast, at high T_e or for ions with small D_0, the Druyvesteyn distribution shifts the maximum of the rate constant of resonant recombination towards higher n, thus allowing for efficient population of highly-excited states of xenon.

For the anisotropic Maxwellian distribution typical of setups with cooled merged beams, we found that the rate constants of the dissociative recombination to the lower Rydberg levels decreased greatly with increase in the detuning energy. As the technique of merged beams is one of the most accurate methods of the measurement of the cross sections and rate constants of various recombination processes, the results of this work should be taken into account when relying upon the data obtained, while using setups with merged beams. Moreover, we showed that the application of the detuning voltage affected the relative roles of the competing channels of dissociative recombination (10) and resonant ternary electron capture (11).

Finally, we note that certain caution is required when using the experimental or theoretical data on the rate constants of the recombination processes in the kinetic modeling of gas and plasma lasers, as well as of the excilamps. While the deviation from the equilibrium EEDFs may seem small; see, for example, Fig. 1; the resulting change in the efficiency of the electron–ion recombination may be substantial.

Acknowledgments

This work was supported by the Russian Science Foundation under Project No. 19-79-30086.

References

1. M. Larsson and A. E. Orel, *Dissociative Recombination of Molecular Ions*, Cambridge University Press (2008).

2. Y. Hahn, *Rep. Prog. Phys.*, **60**, 691 (1997).
3. M. Endo and R. F. Walter, *Gas Lasers*, CRC Press, Boca Raton (2007).
4. Z. J. Mezei, K. Chakrabarti, M. D. E. Epée, et al., *ACS Earth Space Chem.*, **3**, 2376 (2019).
5. W. T. Silfvast, *Laser Fundamentals*, Cambridge University Press (2004).
6. O. Novotný, P. Wilhelm, D. Paul, et al., *Science*, **365**, 676 (2019).
7. X. Jiang, H. Liu, Y. Zhang, et al., *Plasma Sources Sci. Technol.*, **31**, 045016 (2022).
8. L. M. Biberman, V. S. Vorob'ev, and I. T. Yakubov, *Kinetics of Nonequilibrium Low-Temperature Plasmas*, Springer, New York (1987).
9. V. S. Lebedev, K. S. Kislov, and A. A. Narits, *Plasma Sources Sci. Technol.*, **29**, 025002 (2020).
10. V. S. Lebedev, K. S. Kislov, and A. A. Narits, *J. Exp. Theor. Phys.*, **130**, 579 (2020).
11. J. Meichsner, M. Schmidt, R. Schneider, and H.-E. Wagner, *Nonthermal Plasma Chemistry and Physics*, CRC Press, Boca Raton (2013).
12. L. L. Alves, A. Bogaerts, V. Guerra, and M. M. Turner, *Plasma Sources Sci. Technol.*, **27**, 023002 (2018).
13. K. S. Kislov, A. A. Narits, and V. S. Lebedev, *Opt. Spectrosc.*, **128**, 448 (2020).
14. V. S. Zuev, *J. Russ. Laser Res.*, **19**, 23 (1998).
15. S. V. Mit'ko and V. N. Ochkin, *J. Russ. Laser Res.*, **17**, 259 (1996).
16. A. Fridman and L. A. Kennedy, *Plasma Physics and Engineering*, CRC Press, Boca Raton, 2nd ed. (2011).
17. Y. Amemiya, *J. Phys. Soc. Jpn.*, **66**, 1335 (1997).
18. R. A. Phaneuf, C. C. Havener, G. H. Dunn, and A. Müller, *Rep. Prog. Phys.*, **62**, 1143 (1999).
19. L. D. Landau and E. M. Lifshitz, *Quantum Mechanics: Non-Relativistic Theory*, Pergamon, Oxford (1997).
20. O. K. Rice, *J. Chem. Phys.*, **1**, 375 (1933).
21. P. G. Burke and J. Tennyson, *Mol. Phys.*, **103**, 2537 (2005).
22. T. N. Rescigno, C. W. McCurdy, A. E. Orel, and B. H. Lengsfield, "The Complex Kohn Variational Method," in: W. M. Huo and F. A. Gianturco (Eds.), *Computational Methods for Electron–Molecule Collisions*, Plenum Press, New York (1995).
23. V. A. Ivanov, V. S. Lebedev, and V. S. Marchenko, *Sov. Phys. JETP*, **67**, 2225 (1988).